Appl. Phys. B 50, 473–478 (1990)

Applied Physics B Photophysics and Laser Chemistry

Investigation of Flame Structure and Burning Behaviour in an IC Engine Simulator by 2D-LIF of OH Radicals

H. Becker[1], A. Arnold[1], R. Suntz[1], P. Monkhouse[1], J. Wolfrum[1], R. Maly[2], and W. Pfister[2]

[1] Physikalisch-Chemisches Institut der Universität, Im Neuenheimer Feld 253, D-6900 Heidelberg, Fed. Rep. Germany
[2] Daimler Benz AG, Forschung und Technik, Postfach 600 202, D-7000 Stuttgart, Fed. Rep. Germany

Received 15 September 1989/Accepted 8 February 1990

Abstract. Turbulent combustion of propane/air mixtures in an internal combustion engine simulator has been studied by 2D-LIF of OH radicals formed in the combustion process. A laser light sheet of thickness 75 μm at 308 nm was used for excitation of OH and the fluorescence imaged onto an image-intensified CCD-camera. From the large number of images recorded, information on the burning behaviour of various flame structures could be obtained. In particular, flame extinction was clearly observed for lean ($\lambda = 1.5$) mixtures.

PACS: 07.60, 42.30, 82.80

Recent developments in laser diagnostic methods, in particular in two- and three-dimensional imaging techniques, have allowed new insight into the course of turbulent combustion processes as well as the possibility of testing model calculations [1–3]. Both laser-induced fluorescence (LIF) [4–16] and Raman, Rayleigh, and Mie scattering [17–24] have found wide application for this purpose. The LIF method has the advantage over Mie scattering that macroscopic particles are not added to the mixture so that the gas composition is probed directly and no disparity between detected particles and gas flow can occur. Also, the flame front can be imaged sharply. Imaging by LIF for investigating concentration, temperature or velocity fields can be performed either by using transients formed in the combustion process (e.g. OH [4–11], CH [12]) or by doping the combustion mixture with fluorescing molecules (e.g. NO [13], NO_2 [6, 14], I_2 [15], CH_3CHO [16]). The application of 2D-LIF has now been demonstrated in IC engines using OH formed during combustion of propane/air mixtures [4–6]. In our previous work [4], the 0, 0 transition of $OH(X^2\Pi - A^2\Sigma^+)$ at 308 nm was excited using a narrow band, tunable XeCl-laser. The two other recent studies [5, 6] used a dye laser, so that the 1, 0 transition of $OH(X^2\Pi - A^2\Sigma^+)$ near 281 nm could be excited and fluorescence from the 1, 1 band detected. The engines employed in these studies both had a cylindrical cross section rather than the square one employed by us. Both studies used LIF and Mie scattering to identify the location and shape of the flame front although with the two-colour representation used further details of flame structure were not revealed. Schipperijn et al. [6] performed experiments at two different rotation speeds, 300 and 600 rpm, while Felton et al. [5] recorded images for a range of stoichiometries.

We now present new results of OH-LIF-imaging for both stoichiometric and lean mixtures, considering also effects of different ignition and detection times. With the present "engine", detection pressures of up to 14.5 bar were reached. A large number of images were recorded from which information on the burning behaviour of various flame structures and upper limits for the flame front thickness could be obtained. In addition, images taken for lean propane/air mixtures demonstrate flame extinction.

1. Experimental

The experimental set-up for the 2D-measurements was described in detail previously [4]. An excimer laser light sheet (308 nm) was focussed through the quartz side window of the combustion chamber. Fluorescence signals from OH were collected through the top cylinder window with a UV-lens system (Nikon 1:4.5/105 mm) and imaged onto an image-intensified CCD-camera (Proxitronic Nanocam). The gate time used (25 ns) was sufficient to exclude residual flame luminescence. The camera signal was then digitalised by a frame grabber board (Matrox MVP AT) and evaluated by a personal computer (Zenith AT-386).

The XeCl-excimer laser (Lambda Physik EMG 150 EST) was operated in the narrow band mode (FWHM ca. 1 cm^{-1}, tuning range 307.8–308.5 nm, corresponding to the $X^2\Pi - A^2\Sigma^+$, 0,0 transition of OH). By observing the gain profile through the oscillator grating of the laser, the actual line used for excitation was established as being the $Q_1 3$ at 308.154 nm.

The maximum pulse energy was ≈ 300 mJ with a pulse duration of 17 ns. However, the pulse energies actually used were ≈ 25 mJ, corresponding to a spectral intensity of 75 $MW/cm^2 \cdot cm^{-1}$, so that saturation of the OH-fluorescence was avoided, laser stray light markedly reduced and the signal-to-noise ratio improved. The initial dimension of the laser sheet was 25 mm × 10 mm; the sheet thickness of 10 mm was reduced to 75 μm using a series of three quartz cylinder lenses and was constant to $<10\%$ within the detection region.

The transparent engine with its pneumatically driven square piston (Fig. 1) was designed and built by Daimler-Benz, Stuttgart; details are given in Ref. [4]. The square cross section allowed good optical access for the laser light sheet, even near the walls. The cross section was 50 × 50 mm, the stroke 80 mm. The engine was operated in single cycles consisting of intake, compression, and expansion strokes. The combustion chamber was evacuated after each cycle, to remove the exhaust. The piston motion was simulated by an electronically-controlled pneumatic cylinder. The cycle duration lasted ca. 180 ms, corresponding to 500 rpm. Propane/air mixtures were admitted to the engine from a storage tank. In this way OH radicals were detected up to ca. 14.5 bar, with a final burning pressure of 22 bar. However, these pressure limits are set by the engine used, not by the LIF method itself. The temporal variation in the ignition system was determined to be $\approx \pm 0.5$ ms. Compression ratios between 1:4.5 and 1:9 were selected.

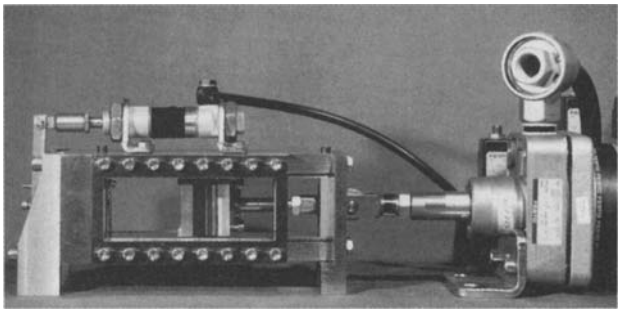

Fig. 1. IC Engine simulator (Daimler Benz). The portion of the combustion chamber detected from the CCD-camera is 10 × 20 mm. The spark plug electrodes are in the centre of the combustion chamber in a plane 6 mm from the cylinder head

2. Results and Discussion

For the 2D-images of OH, a false colour scheme was used to show up areas of different OH concentration. The background was deducted from the images and the residue spread over 256 grey values. The offset due to laser stray light normally took up about 50 grey values. Thus the signal-to-noise ratio was typically in the range 10–20. The temporal resolution is given by the pulse duration (17 ns), which is three orders of magnitude smaller than the scale of flame propagation if a resolution of 75 μm is desired.

Combustion in Stoichiometric and Near-Stoichiometric Mixtures

Figure 2a shows the OH-LIF signal under laminar burning conditions. In this case, the piston is fixed at bottom dead centre and the engine is used simply as a combustion chamber (cf. [11]). The resulting flame front propagates spherically with the laminar front velocity around the ignition electrodes until the walls of the chamber are reached. The area of highest relative concentration includes the actual reaction zone in which the OH radicals are formed (mainly through the reaction $H + O_2 \rightarrow OH + O$). However, at the relatively low detection pressure (1.3 bar) and with the steep OH concentration gradient between reaction zone and unburned fuel, OH radicals diffuse into the unburned zone, leading to a broadened region of increasing OH concentration. Thus the position of the reaction zone is not so sharply defined. Also, at this lower pressure, the OH concentration decreases relatively slowly beyond the flame front towards its equilibrium value because of the lower rates of radical recombination reactions. In fact, in the case of Fig. 2a, the equilibrium OH concentration has not been reached within the section of the image observed.

Figure 2b, recorded at $\lambda = 1$, shows relatively little turbulence (due to the low piston speed). In this case, the propane/air mixture was ignited during the down-

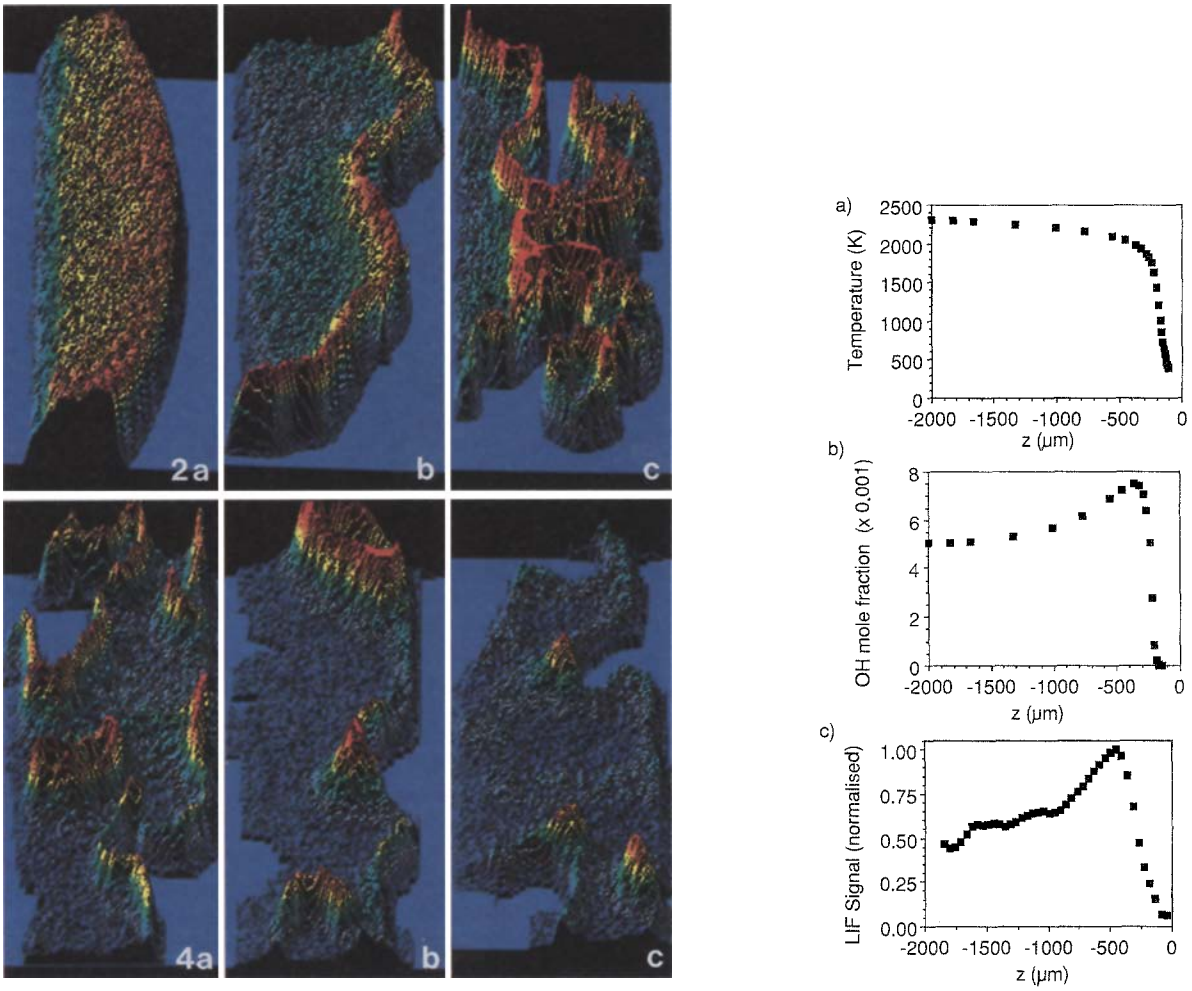

Fig. 2. 2D-LIF of OH Radicals. p_d = detection pressure. (**a**) Laminar flame $\lambda = 1.0$, $p_d = 1.3$ bar; (**b**) compression ratio 4.7, $\lambda = 1.0$, $p_d = 2.7$ bar; (**c**) compression ratio 4.7, $\lambda = 1.4$, $p_d = 5.6$ bar

Fig. 3. (**a**) Calculated temperature profile for the conditions of Fig. 2b; (**b**) calculated OH concentration profile for the conditions of Fig. 2b; (**c**) typical cross section from line profile of Fig. 2b

Fig. 4. Flame extinction for lean ($\lambda = 1.5$) propane/air mixtures. Compression ratio = 9

ward motion of the piston. The detection pressure for this image was about twice that for Fig. 2a, so that diffusion into the unburned zone was slower, radical recombination in the burnt region was faster and the equilibrium OH concentration was established much more rapidly. Thus one observes a much thinner region of highest OH concentration, a more sharply defined reaction zone and an roughly constant OH concentration beyond about 5 mm from the reaction zone. Figure 2c was recorded for $\lambda = 1.4$; in this case the flame burnt more slowly relative to the flow field and was more structured. Here, eddies are present with circumferential speeds greater than the flame speed. Thus these eddies can penetrate into the flame front [3b]; see below.

One-dimensional simulations of propane/air combustion at a pressure of 2.7 bar [24] (the detection pressure of Fig. 2b) give an adiabatic temperature of 2300 K and a maximum mole fraction in the reaction zone of 7.5×10^{-3} at a temperature of 2000 K (see Fig. 3a, b). The equilibrium OH mole fraction, reached at a distance of ≈ 1 cm beyond the reaction zone, is 2.76×10^{-3}, corresponding to 2.5×10^{16} cm^{-3}. Taking a vertical section through the LIF line profile (Fig. 3c) shows that the spatial variation of the relative OH distribution is in qualitative agreement with that of the simulation. From the calculations, the ratio of the maximum to the equilibrium OH concentration is roughly 3 : 1. In the LIF image this corresponds to the transition from the red to the dark blue regions.

The sharp temperature gradient in the flame front leads to a strong change in fluorescence signal in relation to the concentration of particles present. At 1400 K, the OH concentration is about 5% of the maximum concentration (Fig. 3b) and is taken as the threshold for detection. At this temperature, the rotational state from which the excitation takes place ($J''=3.5$) is about 40% more heavily populated than at 2000 K. This leads to a small increase in fluorescence signal at lower temperature relative to the particle concentration and hence to a slight broadening ($\leqq 30$ μm) at the foot of the intensity rise in the line profile.

The high OH number density present in these experiments and the restriction to the very strong 0,0 transition within the tuning range of the XeCl-laser means that self absorption has to be taken into account. The relative population of 0.08 for the $Q_1 3$ rotational level is fairly constant at the steady temperature in the burnt gases. Thus allowing for the broadening (to about 1–2 cm^{-1}) of the rotational lines, one obtains about 35% self-absorption for a path length of 1.3 cm and the equilibrium mole fraction of OH. However, under the turbulent combustion conditions, the absorbing layer is certainly not uniform over the entire image. The thickness of the burnt gas layer between the light sheet and the observation window is known neither for a particular image nor for a section thereof, since propagation varies from image to image and within a single image. Thus the thickness of this layer can be anything between the full distance of 1.3 cm and zero. Also, although the maximum OH concentration is nearly a factor of three higher, this region is extremely thin (<1 mm), so that the average concentration in the region the light sheets traverses is much nearer the equilibrium value. This results in a nearly constant reduction in measured fluorescence intensity so that the form of the profile is not significantly affected.

Another factor which affects the LIF signal is quenching of the excited $A^2\Sigma^+$ state of OH by flame gases (in particular H_2O, CO_2). It has been shown that in the burnt gases of hydrocarbon/air flames at atmospheric and higher pressures, the total quenching rate is essentially constant [25]. For the flame front, it is difficult to estimate the exact effect on the fluorescence intensity, as mole fractions for the flame gases relevant to our conditions are not available. However, as a guide, quenching rates can be estimated using mole fractions [24] calculated for the flame gases and quenching data given by Crosley and Garland [26]. This gives a 25% difference in quenching rate between 1400 K (temperature at the OH detection threshold) and 2000 K (temperature of maximum concentration). Between these two points, of course, the difference becomes progressively less. Thus the net effect on the flame front thickness will be $\leqq 20$ μm.

One must also bear in mind that the angle at which the laser light sheet crosses the flame does not necessarily cross the flame front perpendicularly. If ϕ denotes the angle between flame front and light sheet, the apparent thickness of the flame front exceeds the true thickness by a factor of $1/\sin\phi$. By averaging ϕ over all the spatial directions, with equal probability of all angles, one obtains analytically the probability distribution of the apparent thickness. This shows that 50% of the measured thicknesses deviate by less than 15% from the true value.

The flame front thickness estimated by determining the distance from 10% of the maximum fluorescence intensity to the maximum was $\leqq 300$ μm. This value is larger than the calculated value, 200 μm and the factors discussed above can all contribute to this.

For rotation speeds <1000 rpm, combustion in Otto engines falls in the flamelet region of the Borghi diagram [27]. This diagram shows a logarithmic plot of the ratio of the turbulence intensity v' and the laminar flame velocity v_F as a function of the corresponding ratio of length scales, l_t/l_F. The flamelet region is defined by the following conditions:

– The turbulent Reynolds number,

$$\mathrm{Re}_t = v' \cdot l_t/\nu > 1\,,$$

where l_t is the turbulent length scale, l_F is the laminar flame thickness and ν the laminar viscosity;

– the turbulent Karlovitz number (representing the spatial stretch acting on the smallest eddy in the flame),

$$\mathrm{Ka}_t = l_F^2/l_K^2 < 1$$

where l_K is the length scale for the smallest eddy, i.e. the Kolmogorov scale, and

– the Damköhler number (ratio of the characteristic turbulence and chemical time scales)

$$\mathrm{Da}_t = t_t/t_F = v_F l_t/v' l_F > 1\,.$$

To obtain the characteristic turbulence and flame parameters exactly, flame contours need to be evaluated in detail using Fourier or fractal analysis [3b, 23, 28]. Thus for the present we have limited our discussion to qualitative features directly observable from our results.

Measurements in an IC engine with cylindrical cross section [23] show that the turbulence intensity v' is about half the average piston velocity. In a stoichiometric flame, the laminar flame front velocity is ~ 0.5 m/s, so that for the engine speed of 500 rpm the ratio v'/v_F is near unity.

The speed of eddies of size between l_t and l_K is only sufficient to cause a limited amount of wrinkling in the flame front. As the v'/v_F ratio increases, smaller eddies

will acquire sufficient velocity to penetrate the flame front. The characteristic length scale for the smallest eddy that can penetrate the flame front is termed the Gibson length L_G [3b]. In the region of corrugated flamelets, where interaction between turbulence and combustion is relatively strong, the relation $L_G \sim v_F^3$ holds. In Fig. 2c, the Gibson length is shorter than in Fig. 2b, thus one can observe the effect of smaller eddies penetrating the flame front.

Flame Extinction in Lean ($\lambda = 1.5$) Mixtures

To observe flame extinction, the fuel was ignited about 10 ms after the piston had reached the top dead centre (TDC). In this case the piston moved towards the bottom dead centre (BDC) during the combustion phase. The piston reached BDC at $T \sim 250$ ms. The following general differences between stoichiometric and lean mixtures were found:

Under the same conditions the flame took about three times longer to reach the detection region at $\lambda = 1.5$ compared with $\lambda = 1$. Also, for $\lambda = 1$, the flame burnt towards the walls with increasing detection time whereas for $\lambda = 1.5$ the propagation of the flame front stagnated before the walls were reached.

In the reaction zone, the OH concentration is about the same for the two stoichiometries. However, differences were seen further away from the flame front where the thermal OH concentration, due to the lower temperature, was much lower in the lean than in the stoichiometric flames, compare Fig. 4 with Fig. 2b. No significant differences were found in the flame front thickness for the two mixtures.

Flame extinction can clearly be seen as a disappearing reaction zone in the main parts of Fig. 4a; a reaction zone can only be seen in the centre of three inlets. This is in contrast to Fig. 2b, which was taken with stoichiometric mixtures and still shows a continuous reaction zone. The analysis of 150 images at $\lambda = 1.5$ can be summarized as follows:

- Inlets burned generally better than outlets
- Increments (closed concave structures) burned very well (Fig. 4b and c).
- A continuous bright reaction zone was observed mainly at early detection times. At longer times the reaction zone was absent or less pronounced and discontinuous.

A possible interpretation of these observations is based on the Lewis number, Le (ratio of thermal to mass diffusion). This effect has been investigated numerically for turbulent flow fields in premixed flames [29], whereby contours for the excess or loss of reaction enthalpy were calculated. The results for $Le = 2$ show loss for the leading parts of the flame front, but excess enthalpy for the inlets. Excess enthalpy leads to a local acceleration and hence to a smoothing of the flame front. This result corresponds to our experimental observations for $\lambda = 1.5$ (Fig. 4). However, to evaluate the flame extinction effects fully, systematic flow field measurements and calculations are required and are planned shortly.

3. Conclusions

Using LIF imaging of OH radicals, we have demonstrated imaging of the flame front under turbulent conditions, for stoichiometric and lean propane/air mixtures at detection pressures up to 14.5 bar. For lean mixtures, flame extinction was clearly observed. Qualitative information on flame structure has been obtained. Full interpretation of the data requires further data processing and mathematical evaluation as well as investigations of flow fields and these are in progress. Also underway are 2D-LIF investigations with different excitation and detection schemes with the aim of circumventing quenching and self-absorption. Finally, since the individual length scales depend on the engine speed, measurements over a wide range of speeds are desirable.

Acknowledgements. Funding by the CEC (Project No. EN3E-0056-D (B), "Improved Otto-Cycle") and the BMFT (Arbeitsgemeinschaft TECFLAM, project 6.4 „Hochauflösende Fluoreszenzspektroskopie von OH") is gratefully acknowledged. We also thank G. Ziegler, A. Zettlitz, and J. Köhler of the Institut für Physikalische Elektronik, Universität Stuttgart for technical assistance and Prof. J. Warnatz, Universität Stuttgart for calculating the temperature and concentration profiles.

References

1. W.T. Ashurst, P.K. Barr: Combust. Sci. Tech. **34**, 227 (1983)
2. E.E. O'Brian: In *Turbulent Reacting Flows* ed. by P.A. Libby, F.A. Williams (Springer, Berlin, Heidelberg 1980) p. 185; S.B. Pope: Prog. Energy Comb. Sci. **11**, 119 (1985)
3. a) K.N.C. Bray: In *Complex Chemical Reaction Systems* ed. by W. Jäger, Springer Series in Chem. Phys., Vol. 47 (1987) p. 356; b) N. Peters: 21st Int's Symposium on Combustion, The Combustion Institute (1986) p. 1231
4. R. Suntz, H. Becker, P. Monkhouse, J. Wolfrum: Appl. Phys. B **47**, 287 (1988)
5. P.G. Felton, J. Matzaras, D.S. Bomse, R.L. Woodin: SAE Techn. Paper Ser. (1988) No. 881633
6. F.W. Schipperijn, R. Nagasaka, R.F. Sawyer, R.M. Green: SAE Techn. Paper Ser. (1988) No. 881631
7. M.G. Allen, R.K. Hanson: 21st Int'l Symposium on Combustion, The Combustion Institute (1986) p. 1755; M.G. Allen, R.K. Hanson: Opt. Eng. **25**, 1309 (1986); G. Kychakoff, R.K. Hanson, R.D. Howe: 20th Int'l Symposium on Combustion, The Combustion Institute (1985) p. 1285
8. G. Kychakoff, R.K. Hanson, R.D. Howe: Appl. Opt. **23**, 704 (1984)
9. M.J. Dyer, D.R. Crosley: Opt. Lett. **9**, 217 (1984)

10. R. Cattolica, S. Vosen: Combust. Flame **68**, 267 (1987); Combust. Sci. Technol. **48** (1986)
11. R. Cattolica, S. Vosen: 20th Int'l Symposium on Combustion, The Combustion Institute (1984) p. 1273
12. M.G. Allen, R.D. Howe, R.K. Hanson: Opt. Lett. **11**, 126 (1986)
13. J.M. Seitzman, G. Kychakoff, R.K. Hanson: Opt. Lett. **110**, 439 (1985); G. Kychakoff, K. Knapp, R.D. Howe, R.K. Hanson: AIAA Journal **22**, 153 (1984)
14. R.J. Cattolica: 21st Int'l Symposium Combustion, The Combustion Institute (1988) p. 1551
15. B. Hiller, R.K. Hanson: Appl. Opt. **27**, 33 (1988); B. Hiller, R.K. Hanson: Opt. Lett. **10**, 206 (1985)
16. J. Wolfrum: Appl. Phys. B **46**, 221 (1988); A. Arnold, H. Becker, R. Suntz, P. Monkhouse, J. Wolfrum, R. Maly, W. Pfister: to be published in Opt. Lett.
17. M. Namazian, R.L. Schmitt, M.B. Long: Appl. Opt. **27**, 3597 (1988); M.B. Long, D.C. Fourguette, M.C. Escoda, C.B. Layne: Opt. Lett. **8**, 224 (1983)
18. J.R. Smith: SAE Trans. vol. 91, Paper No. 8220043 (1982) p. 150
19. M.B. Long, P.S. Levin, D.C. Fourguette: Opt. Lett. **10**, 267 (1985); B. Yip, R.L. Schmitt, M.B. Long: Opt. Lett. **13**, 96 (1988); B. Yip, J.K. Lam, M. Winter, M.B. Long: Science **235**, 1209 (1987)
20. P.O. Witze: Exp. Fluids **3**, 174 (1985); P.O. Witze, J.K. Martin, C. Borgnake: Combust. Sci. Technol. **35**, 301 (1984)
21. T.A. Baritaud, R.M. Green: SAE Techn. Paper Ser. No. 860025 (1986); L.D. Chen, W.M. Roquemore: Combust. Flame **66**, 81 (1986)
22. A.O. zur Loye, F.V. Bracco, D.A. Santavicca: Int'l Symposium on diagnostics and modelling of combustion in reciprocating engines, Tokyo (1985) p. 249; J.R. Smith: In *Flames in Internal Combustion Engines* ed. by T. Uzkann (ASME, New York 1983) p. 67
23. G.F.W. Ziegler, A. Zettlitz, P. Meinhardt, R. Herweg, R. Maly, W. Pfister: SAE Techn. Paper (1988) No. 881634; K.N.C. Bray, T.C. Chew, R.R. Maly: Proceedings, Joint Meeting of the British and French Sections, Combustion Institute, Rouen, April 1989; R.R. Maly, T.C. Chew, K.N.C. Bray, W. Pfister, G. Eberspach, K. Geiger: Proceedings, „Motorische Verbrennung", Haus der Technik, Essen, 1989; R.R. Maly, K.N.C. Bray, T.C. Chew: to be published in Combust. Sci. Technology
24. J. Warnatz: private communication
25. R. Schwarzwald, P. Monkhouse, J. Wolfrum: Chem. Phys. Lett. **142**, 15 (1987); J.N. Bergano, P.A. Jaanimagi, M.M. Salour, J.H. Bechtel: Opt. Lett. **8**, 443 (1983)
26. D.R. Crosley, N. Garland: 21st Int'l Symposium Combustion, The Combustion Institute (1988) p. 1693
27. R. Borghi: *Recent Advances in Aeronautical Science* ed. by C. Buro, C. Casci (Pergamon, London 1984)
28. F.C. Gouldin: Combust. Flame **68**, 249 (1987); B.B. Mandelbrot: J. Fluid Mech. **72**, 401 (1975)
29. W.T. Ashurst, N. Peters, M.D. Smooke: Combust. Sci. Tech. **53**, 339 (1987)
30. K.N.C. Bray, P.A. Libby, J.B. Moss: Combust. Sci. Tech. **41**, 143 (1984); K.N.C. Bray, P.A. Libby: Combust. Sci. Tech. **47**, 253 (1986)